Received: 7 November 2019 | Revised: 22 June 2020 | Accepted: 1 August 2020

DOI: 10.1111/jmg.12566

ORIGINAL ARTICLE

Journal of METAMORPHIC GEOLOGY WILEY

EBSD-based criteria for coesite-quartz transformation

Anna K. Bidgood[1] | **Andrew J. Parsons**[1] | **Geoffrey E. Lloyd**[2] | **Dave J. Waters**[1,3] | **Rellie M. Goddard**[1]

[1]Department of Earth Sciences, University of Oxford, Oxford, UK

[2]School of Earth and Environment, University of Leeds, Leeds, UK

[3]Museum of Natural History, University of Oxford, Oxford, UK

Correspondence
Anna Bidgood, Department of Earth Sciences, University of Oxford, South Parks Road, Oxford, UK.
Email: akbidgood@gmail.com

Funding information
Natural Environment Research Council, Grant/Award Number: NE/L002612/1; Royal Geographical Society; Geological Society of London; Mineralogical Society of Great Britain and Ireland; University College, Oxford; Edinburgh Geological Society

Handling Editor: Julia Baldwin

Abstract

Ultra high pressure (UHP) metamorphism observed in continental terranes implies that continental crust can subduct to ~40 kbar before exhuming to the surface. This process is one of the least understood and widely debated parts of the orogenic cycle. The dominantly felsic composition of UHP continental terranes means that many petrology-based techniques for determining peak pressures and temperatures are often not possible. In such cases, the detection of UHP conditions depends on the preservation of coesite, a rarely preserved mineral in exhumed UHP terranes as it rapidly transforms to quartz on decompression. Consequently, the qualitative identification of palisade quartz microstructures that form during the retrograde transformation of coesite to quartz is often used to identify UHP terranes. In this study, we conduct electron backscatter diffraction and misorientation analysis of palisade quartz inclusions in the coesite-bearing pyrope quartzite from the Dora Maira massif in the Alps, and matrix-scale palisade quartz in the Polokongka La granite from Tso Morari in the Ladakh Himalaya, in order to quantitatively define crystallographic characteristics of quartz after coesite. The repeatability of our observations in two unrelated occurrences of UHP rocks supports our interpretation that the following features provide a systematic and predictable set of criteria to identify the coesite to quartz transition: (1) Quartz crystallographic orientations define spatially and texturally distinct subdomains of palisade quartz grains with 'single crystal' orientations defined by distinct *c*-axis point maxima. (2) Adjacent subdomains are misorientated with respect to each other by a misorientation angle/axis of 90°/<*a*>. (3) Within each subdomain, palisade quartz grain boundaries commonly have intra- and inter-granular misorientations of 60°/[0001], consistent with the dauphiné twin law. Our observations imply that the coesite-quartz transformation is crystallographically controlled by the epitaxial nucleation of palisade quartz on the former coesite grain, specifically on potential coesite twin planes such as (−101) and (021).

KEYWORDS

coesite, electron backscatter diffraction, palisade, quartz, ultra high pressure

1 | INTRODUCTION

Ultra high pressure (UHP) conditions have been proposed in continental terranes such as the Alps (Chopin, 1984), the Himalaya (Sachan et al., 2004), the Norwegian Caledonides (Smith, 1984) and the Dabie-Sulu region (Okay, Xu, & Sengor, 1989). Such occurrences continue to drive debate over the extent and mechanisms by which continental crust may be subducted and exhumed during continental collision (e.g. Hacker & Gerya, 2013; Parsons, Hosseini, Palin, & Sigloch, 2020; Warren, 2013), and the importance of this process for orogenic cycles (e.g. Afonso & Zlotnik, 2011; Capitanio, Morra, Goes, Weinberg, & Moresi, 2010). The dominantly felsic composition of UHP continental terranes means that standard petrology-based techniques for determining peak pressures and temperatures are often not possible (e.g. O'Brien, 2018). In such cases, evidence for subduction to UHPs is entirely dependent on the identification of coesite (Chopin, 1984; Smith, 1984). However, the low preservation potential of coesite, which rapidly transforms to quartz on decompression (Perrillat, Daniel, Lardeaux, & Cardon, 2003), makes detection of UHP conditions in felsic rocks extremely difficult (e.g. Palin, Reuber, White, Kaus, & Weller, 2017), and direct evidence of coesite is mostly preserved as rare inclusions within minerals in mafic rocks (e.g. Wain, 1997). Here, we document previously unreported crystallographically constrained quartz microstructures that define transformation of coesite to quartz in two unrelated occurrences of UHP metamorphism. The first is reported from the Dora Maira pyrope quartzite in the Alps. The second is reported from a granite in the Tso Morari UHP dome in Ladakh, NW Indian Himalaya. With respect to our analysis of the Tso Morari granite, these microstructures support previous studies that argue for subduction of Indian continental crust to UHPs at onset of the Himalayan orogeny (O'Brien, 2006; O'Brien, Zotov, & Law, 1999; St-Onge, Rayner, Palin, Searle, & Waters, 2013).

Palisade quartz as a replacement of coesite was originally recognized in the pyrope quartzite of the Dora Maira massif in the western Alps (Chopin, 1984). In those rocks, palisade quartz forms a rim of radially arranged elongate grains surrounding coesite inclusions within garnet and kyanite (Schertl, Schreyer, & Chopin, 1991). Schertl et al. (1991) also observed matrix palisade quartz in embayments into garnet and in quartz bands separated by folia of coarse-grained phengite (e.g. Figure 1a). These palisades were inferred to form by nucleation and growth of quartz from the margins of the bands inwards, from the external boundary of coesite domains towards a central medial line (Lenze & Stöckhert, 2008), similar to the formation of syntaxial veins. However, the specific formation mechanisms of palisade quartz textures are poorly understood, and their identification based purely on qualitative criteria.

A study by Langenhorst and Poirier (2002) using transmission electron microscopy (TEM) suggested that there is a crystallographic control on the coesite to quartz transformation. They observed quartz veins aligned parallel to (100) and (021) composition planes of twins in coesite, suggesting that quartz nucleating after coesite starts at grain and twin boundaries. By contrast, other studies using electron backscatter diffraction (EBSD) techniques (Lenze & Stöckhert, 2007, 2008) proposed that the crystallography of coesite has no control over the nucleation and growth of quartz, owing to an apparently random orientation of palisade quartz after

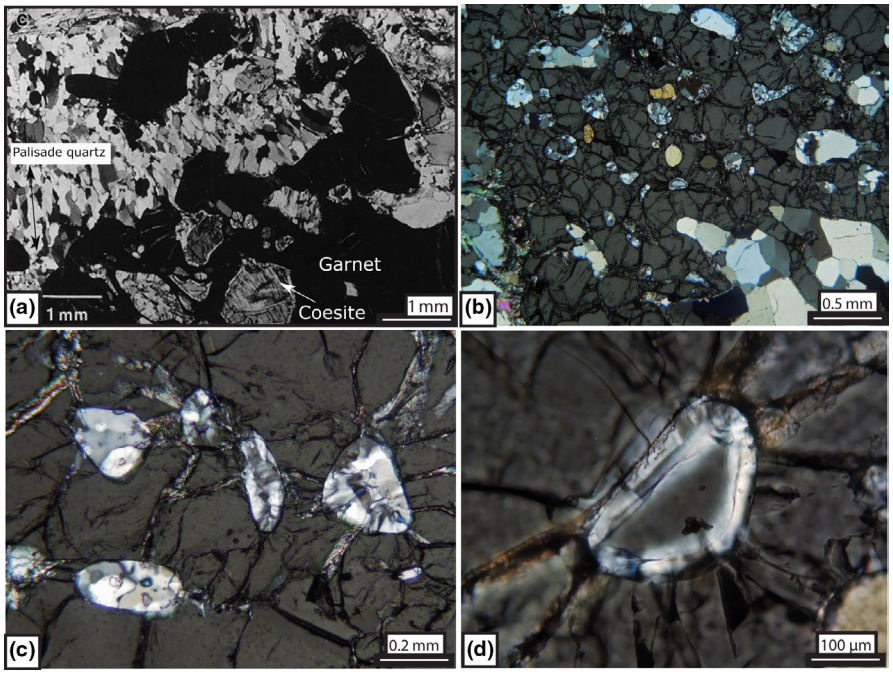

FIGURE 1 (a) Photomicrograph of the Dora Maira Pyrope Quartzite from Schertl et al. (1991). Palisade quartz textures are replacing high relief coesite inclusions in garnet (isotropic) and coarser palisade quartz textures are preserved in the matrix, oriented perpendicular to quartz–garnet interface. (b, c) Photomicrographs of sample DW09-53 showing palisade textures in polycrystalline quartz inclusions in garnet. (d) Photomicrograph of coesite inclusion surrounded by palisade quartz texture included in garnet with radial fractures [Colour figure can be viewed at wileyonlinelibrary.com]

coesite. However, these studies did not investigate the domainal fabric and grain boundary misorientation of quartz palisade microstructures, as proposed in this study, and the presentation of uncontoured pole figures makes quantitive interpretation and comparison of crystallographic orientations difficult.

We present new petrographic, EBSD, and misorientation analyses of palisade quartz surrounding a relict coesite inclusion in garnet from the Dora Maira Pyrope Quartzite (e.g. Lenze & Stöckhert, 2008; Schertl et al., 1991) and palisade quartz in the matrix of a granite from the Tso Morari complex, in order to investigate the crystallographic relationships of the coesite–quartz transformation. We present the first detailed misorientation analysis of palisade quartz, from which we document several previously unreported textural observations, including domains of quartz palisade grains with systematic crystallographic orientations and grain boundary misorientations. Based on the reoccurrence of systematic quartz crystallographic preferred orientations and grain boundary misorientations observed in both the Dora Maira and Tso Morari examples, we suggest that the nucleation of quartz during the coesite-to-quartz transformation is crystallographically controlled. We propose that our reported observations define a quantitative set of predictable criteria for identifying UHP conditions in the absence of coesite, which is independent from other mineral chemistry-based barometers. We attribute the preservation of these microstructures to the relatively undeformed nature of the host rock in the case of the Tso Morari sample, and the shielding of quartz by the surrounding garnet in the case of the Dora Maira sample, and postulate that similar crystallographic relationships may exist between quartz palisade grains in other UHP terranes yet to be investigated via EBSD misorientation analysis.

2 | METHODS

Quartz microstructures were initially investigated by optical microscopy of polished thin sections (30 μm thick). The quartz crystal preferred orientations (CPOs) were subsequently determined using EBSD collected on an FEI Quanta 650 FEG E-Scanning electron microscope equipped with Oxford Instruments Aztec (version 3.3) acquisition software and a NordlysNano EBSD camera. The sample was mapped at low vacuum (50 Pa, H_2O), tilted to 70°, with an accelerating voltage of 30 kV and a working distance of 15 mm. In order to reduce mapping times, step sizes of 20 μm were used and Kikuchi patterns were binned (2 × 2 binning).

EBSD data were processed using the MTEX package for MATLAB (Bachmann, Hielscher, & Schaeben, 2010; Mainprice, Bachmann, Hielscher & Schaeben, 2014), which was also used to create and analyse crystal orientation pole figures as well as All-Euler and band contrast maps. Isolated pixels and small grains ≤5 pixels were removed. Non-indexed points surrounded by ≥6 indexed points were given the average orientation of their neighbours using the smoothing spline filter.

Crystal axes and poles to crystal planes are plotted on pole figures with lower hemisphere projections and contoured in units of multiples of uniform distribution (m.u.d.) using an orientation density function. Quartz pole figures were constructed for <*a*> and [*c*] crystallographic axes, and {*r*} and {*z*} poles to planes. The <*a*> axes were plotted as antipodal projections to avoid being plotted on opposite hemispheres. Subsets of quartz crystallographic orientation data with common orientations presented in Figures 5–7 were extracted from each data set by selecting orientations within 5° of statistically defined modal orientations. Coesite pole figures were constructed for the *a*[100], *b*[010] and *c*[001] axes and (100), (010), (001), (021), (02−1), (−101) poles to planes (Table 1).

3 | PYROPE QUARTZITE, DORA MAIRA MASSIF

3.1 | Geological Setting

Sample DW09-53 (7.332°E, 44.592°N) is a pyrope–phengite–quartz schist from the UHP Brossasco–Isasca unit in

TABLE 1 Coesite and quartz poles to planes and crystallographic axes. Potential twin planes in coesite (Langenhorst & Poirier, 2002; Schertl et al., 2005) are marked in bold

Coesite—monoclinic	Quartz—trigonal
[*a*] [100]	[*c*] [0001]
[*b*] [001]	<*a*> [−2110]
	[−12−10]
	[11−20]
	[2−1−10]
	[1−210]
[*c*][010]	{*r*} (10−11)
	(0−111)
	(−1101)
(100)	{*z*} (−1011)
	(1−101)
	(01−11)
(010)	
(001)	
(021)	
(02−1)	
(−101)	

the southern part of the Dora Maira massif, on the northern side of the Val Gilba in the Italian Western Alps (e.g. Compagnoni & Rolfo, 2003; Compagnoni, Rolfo, Groppo, Hirajima, & Turello, 2012). The Dora Maira massif contains slices of continental crust, which have experienced UHP conditions (e.g. Avigad, Chopin, & Le Bayon, 2003). The UHP mineral assemblages in its constituent lithologies (e.g. eclogites, marbles, metagranites and the pyrope quartzite) indicate peak metamorphic conditions of ~35–42 kbar and 730–830°C (Chopin & Schertl, 1999; Gebauer, Schertl, Brix, & Schreyer, 1997; Schertl et al., 1991). The pyrope quartzite is a coarse-grained rock with 3–4 mm compositional layering defined by quartz- and phengite-rich domains with poikilitic pyrope garnet present in the matrix and is now regarded as a type of whiteschist formed by the metasomatic transformation of the surrounding granitic rocks (e.g. Chopin, 1984; Chopin & Schertl, 1999; Gebauer et al., 1997; Philippot, Chevallier, Chopin, & Dubessy, 1995; Schertl et al., 1991). Coesite is observed as inclusions in coarse poikiloblastic garnet, often surrounded by fine-grained radially arranged palisade quartz grains with a 'feathery' texture (Schertl et al., 1991).

3.2 | Sample Petrography

Palisade quartz grains surrounding coesite inclusions in garnet, in sample DW09-53, are typically 20–50 μm in length and ~5–20 μm in width (Figure 1b–d), oriented perpendicular to the host boundary. Intracrystalline deformation features in these grains are not visible using optical microscopy owing to the fine grainsize. However, EBSD disorientation maps (Figure 2b), which plot the orientation within each grain, relative to a reference point (cf. Germain, Kratsch, Salib, & Gey, 2014), indicate subtle lattice strain textures in the palisade quartz similar to textures seen in the host garnet. In contrast, coesite exhibits no such features.

Quartz grain boundaries are commonly planar with smaller equant recrystallized grains, ~5 μm in diameter, occurring between regions of corresponding EBSD Euler colours (Figure 2a). Sample DW09-53 also shows embayments of elongate palisade quartz grains encroaching on an included single coesite grain forming a lobate quartz–coesite boundary (Figure 2a). Palisade quartz is visible in the matrix forming ~5 mm long, 2–3 mm wide quartz grains (Figure 1a), often spanning foliation-parallel compositional bands between phengite grains.

3.3 | Crystallographic preferred orientation and grain boundary misorientation analysis

In the pyrope quartzite sample, palisade quartz grains surrounding an inclusion of coesite within garnet were analysed. The coesite inclusion forms a single crystal with a sub-horizontal [001] axis with a south–southeast azimuth in sample coordinates (Figure 3a). Radially arranged palisade quartz surrounds and encroaches on the coesite (Figure 2a) suggesting that the quartz nucleated on the coesite grain boundaries and grew inwards, away from the garnet-inclusion interface. Within the radially arranged palisade quartz, crystallographic axis orientations are organized into multiple 'single crystal' populations, each defined by a distinct point maximum of *c*-axis orientations (Figure 3g–h). Each 'single crystal' population of *c*-axis orientations defines a texturally and spatially distinct subdomain comprised of several quartz grains (Figure 3c–e).

Within each subdomain, the *c*-axis point maximum and apparent grain-shape long axes are orientated perpendicular or parallel to the adjacent inclusion boundaries. In each subdomain irregular intragranular boundaries with misorientations of 60°/[0001] (red lines in Figure 2a), form typical intragranular dauphiné-twin relationships. This is consistent with the orientations of *r*- and *z*-planes ({10−11} and {01−11} respectively), which form six point maxima around a single *c*-axis point maximum (Figure 3f–h), rather than the conventional three point maxima displayed by a single crystal of quartz (Figure 6g–h). Populations of 'single crystal' *c*-axis orientations from adjacent subdomains are misoriented by ~90°/<*a*> with respect to each other (Figure 3b). This is observed in multiple adjacent domains around a single coesite inclusion. Quartz 'single crystal' *c*-axis orientations from subdomains 1 and 2 lie along a great circle parallel to the (101) plane (Figure 3b—yellow great circle) of the coesite inclusion and are evenly bisected by the (−101) plane of the coesite inclusion (Figure 3b—dashed yellow great circle).

4 | POLOKONGKA LA GRANITE, TSO MORARI

4.1 | Geological Setting

Sample a05-10 (78.1882°E, 33.2465°N) is a macroscopically undeformed metagranite from the Polokongka La region in the central part of the UHP Tso Morari complex, on the northern margin of the Indian plate in the Ladakh Himalaya (e.g. Epard & Steck, 2008; Girard & Bussy, 1999). The Tso Morari dome contains a stack of thrust units, the lowermost of which, the Tso Morari complex (equivalent to the Tso Morari nappe of Epard & Steck, 2008), comprises a core of Ordovician granitic gneiss and a carapace of Palaeozoic to Mesozoic metasedimentary rocks (Supporting Information 1). The metasedimentary rocks are part of the Tethyan Himalaya sequence that formed part of the leading edge of the Indian continent prior to the Himalayan orogeny (Steck et al., 1998). Within this nappe, eclogite facies mineral

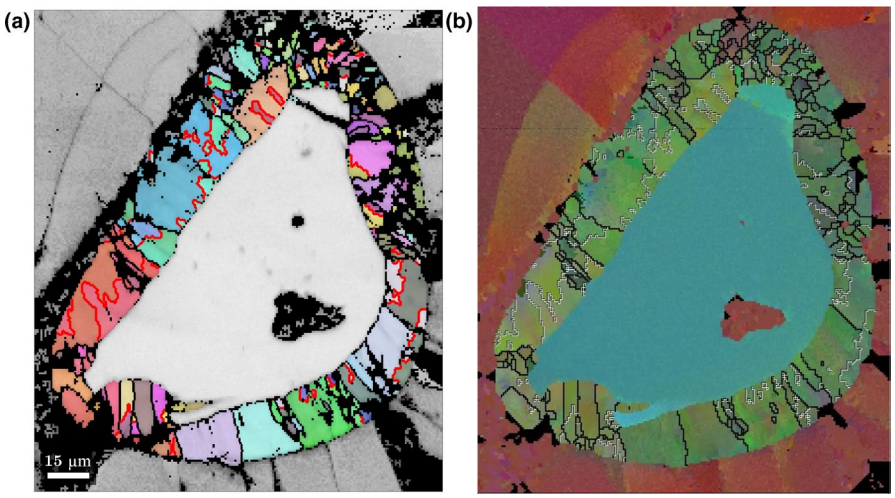

FIGURE 2 Sample DW09-53A from the Dora Maira Pyrope Quartzite. (a) Quartz All-Euler map of coesite and palisade quartz included in garnet. Misorientations of 60°/[0001] are shown as red lines. (b) Quartz disorientation map which plots the orientation within each phase relative to a reference point. Regions with a similar orientation with respect to the reference point plot as similar colours. Grain boundaries (>10° misorientation) shown as black lines. Misorientations of 60°/[0001] are shown as white lines [Colour figure can be viewed at wileyonlinelibrary.com]

assemblages associated with subduction of the Indian continental crust have been extensively overprinted at amphibolite facies, but are locally preserved in sparsely distributed mafic boudins, hosted in both granitic gneiss and metasedimentary rocks (Guillot, De Sigoyer, & Lardeaux, 1997).

Thermobarometric estimates from mafic eclogites (e.g. Sigoyer, Guillot, Lardeaux, & Mascle, 1997; St-Onge et al., 2013), and the discovery of coesite inclusions in garnet rim zones within mafic eclogite boudins (Sachan et al., 2004), suggest that the mafic rocks experienced UHP conditions of over 26 kbar (O'Brien, 2006; O'Brien et al., 1999; St-Onge et al., 2013) (Supporting Information 3). Evidence for eclogite facies metamorphism in the abundant felsic rocks of the Tso Morari dome is limited to rare observations of eclogite facies mineral assemblages preserved in metasedimentary rocks (Guillot et al., 1997) and evidence of partial transformation of primary igneous phases in low-strain metagranites (Bidgood, Waters, Searle, Roberts, & Ahmad, 2018). However, the broad distribution within felsic rocks of mafic pods with evidence for eclogite facies metamorphism suggests that the entire Tso Morari nappe subducted to eclogite facies conditions.

Deformation in the Tso Morari complex is highly heterogeneous, and local areas of undeformed granite grade laterally into strongly deformed orthogneissic mylonites (Epard & Steck, 2008; Girard & Bussy, 1999). The centre of the Tso Morari complex comprises a 10 × 5 km region of variably metamorphosed but macroscopically undeformed granite, known as the Polokongka La granite (Berthelsen, 1953; Thakur, 1983), and is surrounded by the Puga Gneiss, an orthogneiss with the same protolith as the Polokongka La granite (Girard & Bussy, 1999). Exposures of the Polokongka La granite crop out along mountain ridge tops, which are surrounded by a shattered landscape of granite boulders and occasional retrogressed mafic eclogite boulders (Figure 4f).

4.2 | Sample Petrography

Sample a05-10 was collected from a boulder on top of a ridge, which is located within a 5 km wide granite boulder field surrounded by >6,000 m high mountains of Puga Gneiss. The angular geometry and large size of these granite boulders combined with the lack of evidence for fluvial processes suggest that they derive locally from the Polokongka La granite (Figure 4f). This granite has an assemblage of quartz, K-feldspar, biotite and white mica, with fine-grained domains of phengite+albite and phengite+garnet+kyanite that pseudomorph igneous plagioclase and cordierite respectively (e.g. Figure 4a,b). Quartz in the granite typically occurs as distinct, 3–4 mm euhedral relict igneous grains (Figure 4c), or as aggregates of recrystallized quartz that have collectively retained the original shapes of igneous quartz grains, as defined by surrounding feldspar domains (Figure 5a–e). Some quartz grains exhibit synneusis, indicative of crystallization early in the magmatic history (Figure 4c).

Sample a05-10 contains isolated domains of recrystallized quartz grains (Figure 5a–e); comparison with other undeformed granite samples collected from this region suggests that these recrystallized quartz domains originally formed as a single igneous quartz crystal (c.f. Figure 4). Many of these recrystallized quartz domains preserve palisade textures, which consist of elongate grains spanning the domains. The elongate recrystallized grains are ~0.5–2 mm in length and

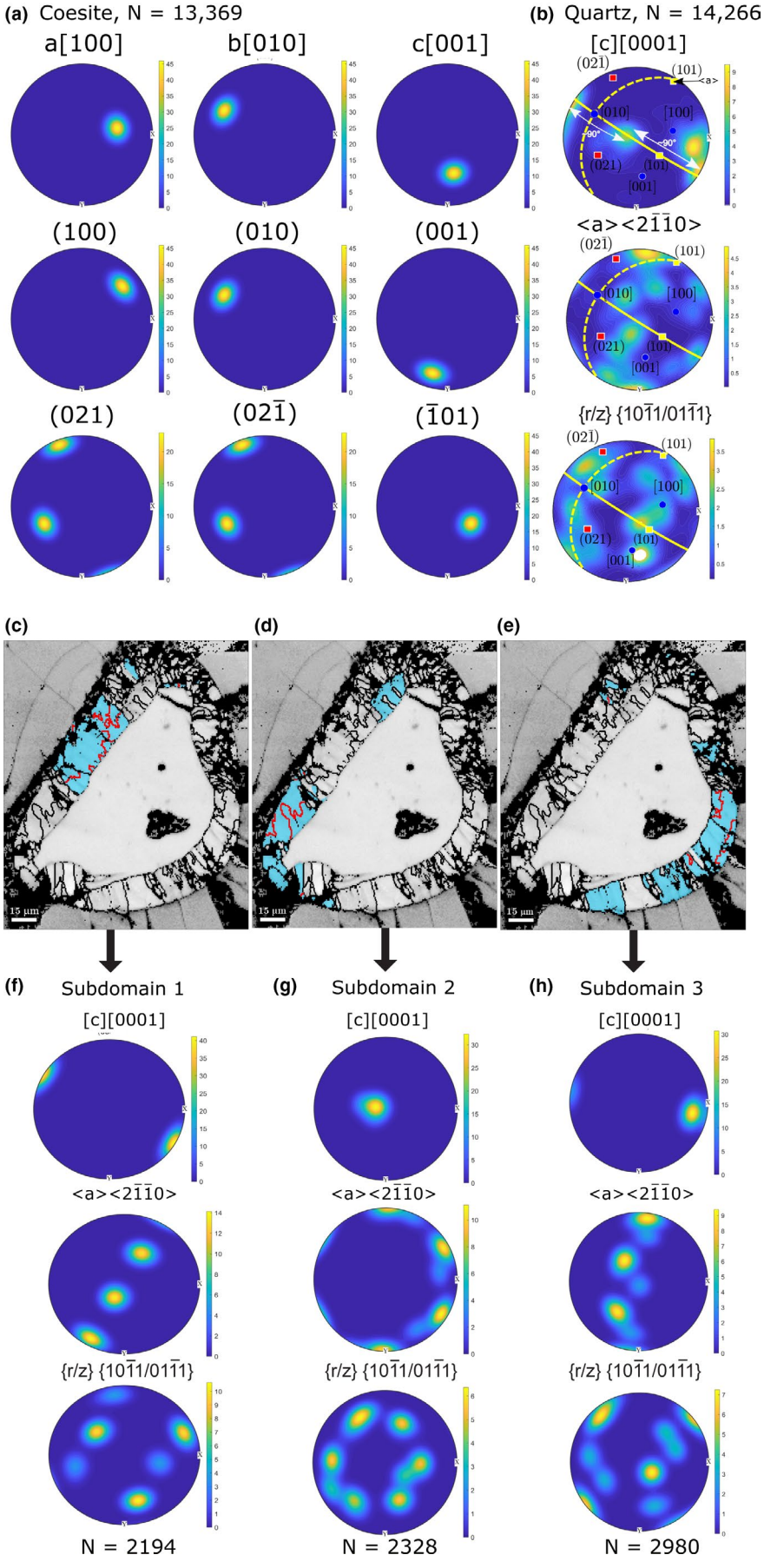

FIGURE 3 Sample DW09-53A from the Dora Maira Pyrope Quartzite. All pole figures are lower hemisphere projections. Step size is 1 µm. (a) Coesite pole figures. (b) Quartz pole figure showing multiple *c*-axis clusters within the data set oriented at 90°/<*a*>. Coesite crystallographic axes, planes and pole to planes are overlain on the quartz pole figure. Coesite axes are plotted as blue circles. Poles to planes plotted as squares, with corresponding planes plotted as great circles of the same colour. (101) solid yellow line, (−101) dashed yellow line. The common a-axis of quartz *c*-axis clusters is indicated and corresponds to the (101) coesite pole to plane. (c–e) Quartz grain map showing the grains which corresponds to the c-axis orientations below. (f–h) Subsets defined by *c*-axis clusters corresponding to grains above [Colour figure can be viewed at wileyonlinelibrary.com]

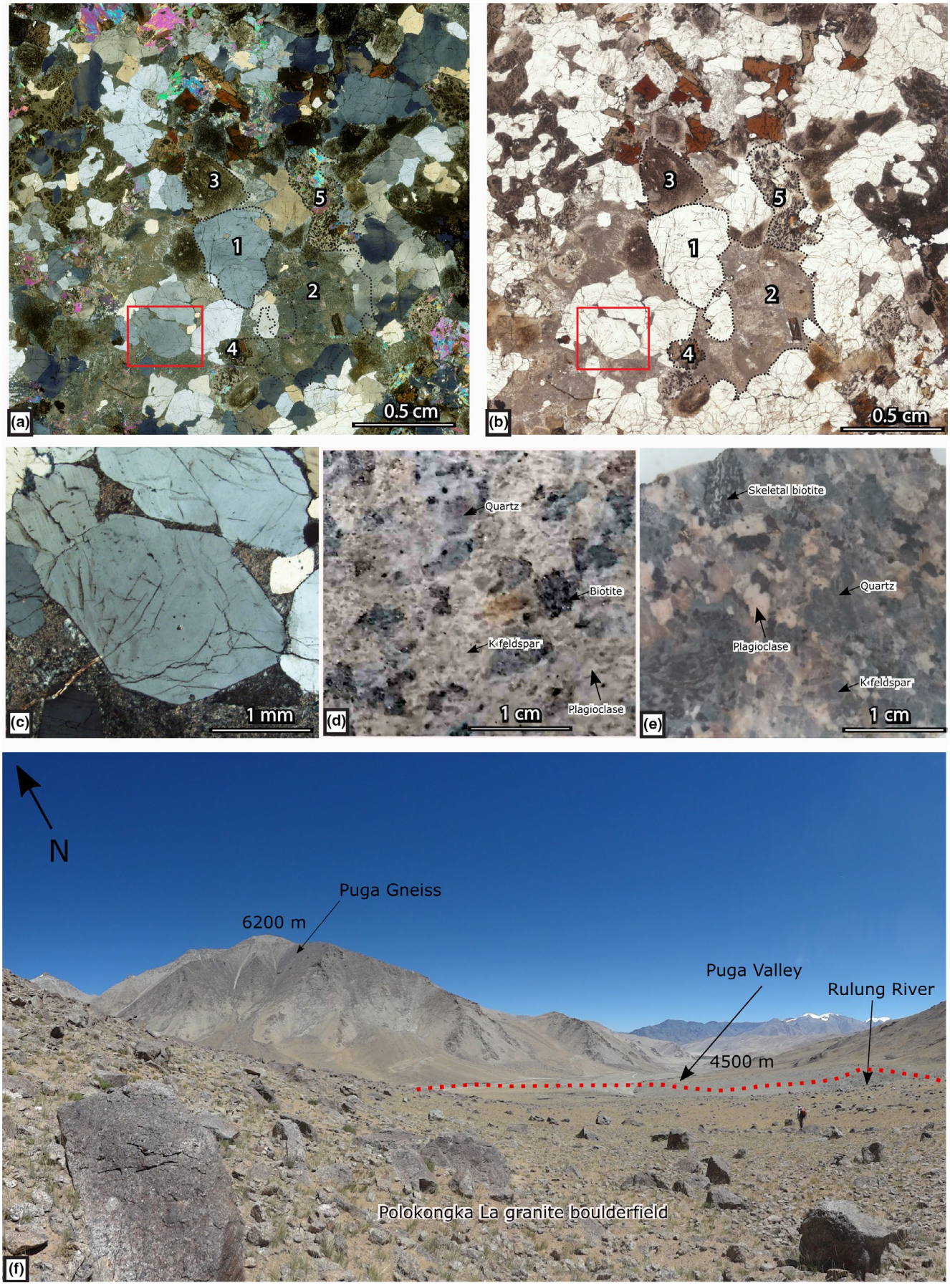

~0.2–0.3 mm in width and have a strong grain-shape alignment of grain long axes observed across the thin-section. Intracrystalline deformation features in these grains include undulose extinction and tabular subgrains oriented subparallel to the quartz grain-shape long axis. The grain boundaries are commonly lobate, on a scale of 0.05–0.1 mm. Smaller equant recrystallized grains, ~0.05–0.1 mm in diameter, also occur in the quartz domains and are interpreted to have formed by dynamic recrystallization of elongate grains (e.g. Passchier & Trouw, 2005), post-dating the formation of the palisade grains.

4.3 | Crystallographic preferred orientation and grain boundary misorientation analysis

In the Polokongka La granite sample, several matrix domains of palisade quartz grains were analysed (Figure 6); each domain is interpreted to have developed via recrystallization from a single igneous quartz grain. There does not appear to be any systematic relationship between quartz crystallographic and/or grain-shape orientations from different quartz domains. Within each domain of recrystallized quartz, crystallographic axis orientations are organized into at least two 'single crystal' populations, each defined by a distinct point maximum of *c*-axis orientations (Figure 7a,d). Each population of *c*-axis orientations derives from a texturally and spatially distinct subdomain of the larger encompassing domain (Figure 7b,c). Within each subdomain, the trace of the *c*-axis point maximum is orientated subparallel to the apparent grain-shape long axes (Figure 7b,c). In each subdomain, grain boundary misorientations of 60°/[0001] (i.e. red lines on Figures 6a–c and 7) are recorded along optically identified palisade quartz grain boundaries and within the palisade grains. These intragranular misorientation boundaries are not optically visible and typically have an irregular boundary trace. Like the Pyrope Quartzite example, inter- and intragranular misorientations of each subdomain produce six point maxima of *r*- and *z*-poles to planes ($\{10\bar{1}1\}$ and $\{01\bar{1}1\}$ respectively) around a single *c*-axis point maximum, consistent with the dauphiné twin law (Figure 7e–h). Also like the pyrope quartzite example, populations of *c*-axis orientations from adjacent subdomains in the Polokongka La sample are misoriented by ~90°/<*a*> with respect to each other (Figure 7d). Boundaries between these subdomains bisect the encompassing quartz domain.

5 | DISCUSSION

Electron backscatter diffraction analysis of palisade quartz in the pyrope quartzite and Polokongka La granite has revealed the following crystallographic relationships, which are common to both samples: (1) quartz crystallographic orientations form multiple populations with 'single crystal' orientations defined by distinct *c*-axis point maxima; (2) Each 'single crystal' population of orientation measurements defines a spatially and texturally distinct subdomain of palisade quartz grains; (3) within each subdomain, the *c*-axis point maximum orientation is generally subparallel to the apparent grain boundary orientation of the palisade quartz grains in that subdomain; (4) within each subdomain, misorientations of 60°/[0001] are recorded along irregular intragranular boundaries, whereas *r*- and *z*-poles to planes each form six point maxima around a single *c*-axis orientation; (5) adjacent subdomains are misoriented with respect to each other by a misorientation angle/axis pair of 90°/<*a*>; and (6) all *c*-axis point maxima from a single domain fall on a great circle that is approximately perpendicular to the <*a*> axis. In addition to the above commonalities, in the pyrope quartzite sample, the trace of the quartz *c*-axis point maxima orientations and palisade grain boundaries is either perpendicular (subdomains 1 and 3) or parallel (subdomain 2) to adjacent inclusion boundaries.

With respect to the Polokongka La granite sample from Tso Morari, we suggest that the palisade quartz grains formed from complete transformation of original igneous quartz grains to coesite, followed by complete coesite-to-quartz reverse transformation during decompression. In this sample, each domain of palisade quartz corresponds to a single igneous quartz grain from the protolith (Figure 5c–e). Within each domain, the boundary between subdomains bisects the outline of the former igneous quartz. Individual domains in this sample have different and unrelated crystallographic orientations, suggesting that the 'single crystal' CPOs within each domain did not form in response to deformation-driven dynamic recrystallization, as this would produce a shared

FIGURE 4 (a, b) Photomicrograph of granite from Tso Morari dome, Sample 11-01 showing representative domains with igneous textural relationships. 1. Quartz domain, 2. K-feldspar domain partially pseudomorphed by white mica, 3. Plagioclase domain pseudomorphed by white mica+albite, 4. White mica and biotite domain, 5. Cordierite domain pseudomorphed by garnet, phengite, phlogopite and kyanite. Red box shows texture shown in (c). (c) Sample 11-01, photomicrograph of red box in (a) and (b) showing a cluster of euhedral quartz grains with face contacts. (d) Sample a05-10 coarse-grained granite texture in hand specimen. (e) Sample a12-01, granite texture in hand specimen with skeletal biotite domains. (f) Photograph showing boulder field that marks the extent of the Polokongka La granite (red dotted line) within the Tso Morari complex. >95% of boulders consist of macroscopically undeformed granite within this region. Hills on the north side of the Puga Valley composed of Puga Gneiss with boudins of low-strain metagranites. Sparse rocky outcrops occur along the ridge tops and sides. View looking NE along Puga Valley with Rulung river running SW (right of frame) [Colour figure can be viewed at wileyonlinelibrary.com]

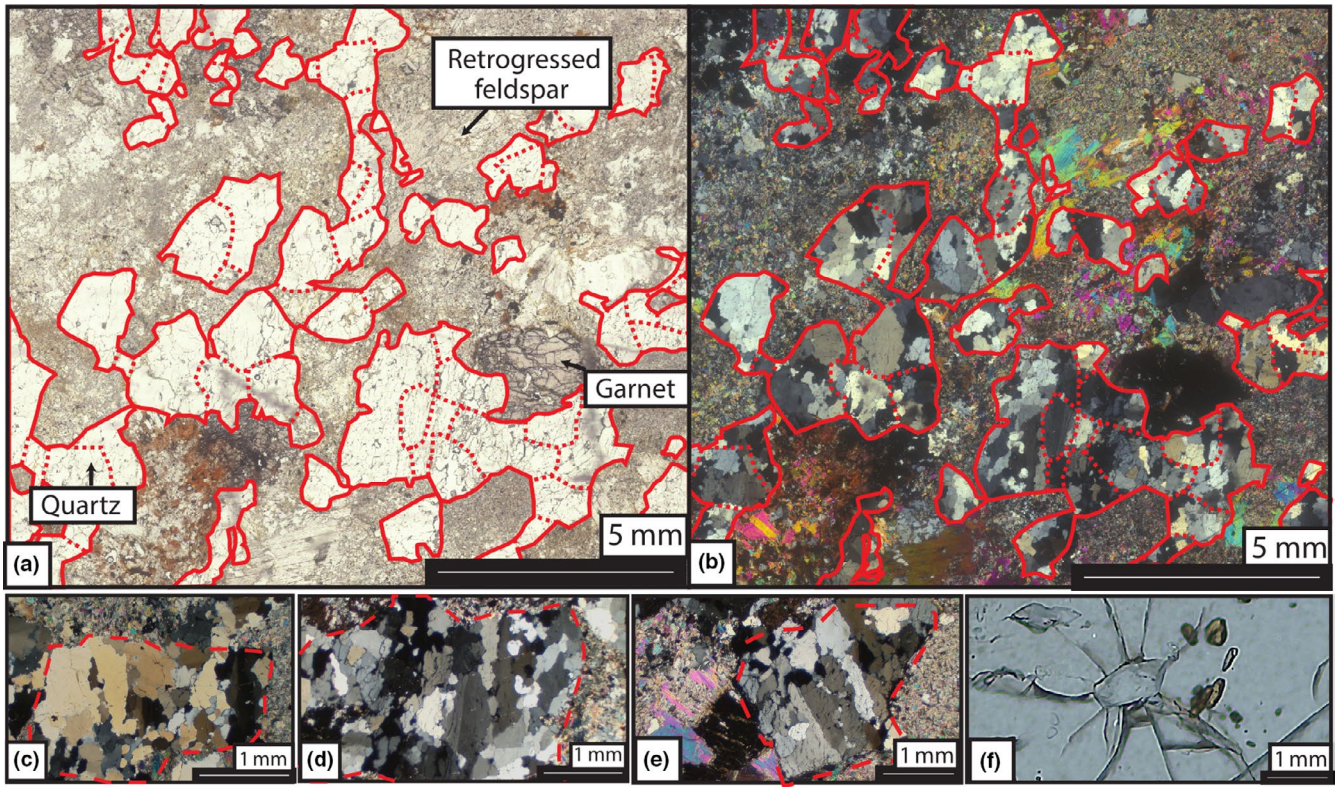

FIGURE 5 Sample a05-10 is a garnet-bearing granite boulder taken from the Polokongka La region of the Tso Morari dome, which forms an area of ~1 km^2 undeformed granite outcrop, 78.1882°E 33.2465°N (see Figure 3). Photomicrographs a. and b. of sample a05-10 show distinct quartz domains outlined with solid red lines, corresponding to single igneous quartz grains or quartz clusters surrounded by fine-grained mica aggregates, representing the original feldspar domains (Bidgood & Waters, 2019). Clusters of quartz grains with a common extinction angle are subdivided by dotted red lines. Palisade quartz textures extend across the quartz domain. Intracrystalline deformation is present within the palisades. Grain boundary migration and subgrain formation is dominant along the grain boundaries of the palisades. (c–e) Photomicrographs of sample a05-10 showing palisade quartz textures confined to quartz domains outlined by the red dotted lines. (f) Photomicrograph of a polycrystalline quartz inclusion in garnet surrounded by radial fractures from sample 05-04, a mafic eclogite in the Tso Morari dome, 78.3610°E 33.1627°N [Colour figure can be viewed at wileyonlinelibrary.com]

crystallographic preferred orientation common to all domains. These sample-wide observations are consistent with the findings of Lenze and Stöckhert (2008) who observed no common quartz CPO across their sample. In their study, Lenze and Stöckhert (2008) interpreted the CPO of palisade quartz as randomly orientated when plotted for a region of matrix quartz and for polycrystalline quartz inclusions; however, they did not investigate domainal fabrics or grain boundary misorientation of quartz palisade microstructures as described in our study.

Based on the repeatability of the observations in the pyrope quartzite of the Dora Maira massif, and the Polokongka La granite of the Tso Morari complex, we argue that the above listed crystallographic orientation and misorientation features define a systematic (i.e. predictable) crystallographic control on the nucleation of palisade quartz from coesite. We suggest that these observations may be used as a quantitative set of criteria for identifying the former presence of coesite in quartz rich rocks in the absence of coesite, which is independent of other mineral chemistry-based barometers.

5.1 | Crystallographically controlled nucleation of quartz from coesite

In both samples, palisade quartz grain-shape long axes are orientated subparallel to the trace of the *c*-axis point maximum of their corresponding subdomain, suggesting preferential nucleation and growth of quartz in the *c*-axis direction (e.g. Hippert, 1994; Ihinger & Zink, 2000). Within each subdomain, misorientations of 60°/[0001] are recorded along intragranular irregular boundaries in both samples that cannot be observed via transmitted light microscopy, as well as along straight, optically visible palisade grain boundaries in the Polokongka La sample (red boundary lines in Figures 6 and 7). These irregular intragranular misorientation boundaries are consistent with a dauphiné twin relationship (Green, Griggs, & Christie, 1970; Tullis, 1970), which is defined by a 180° (equivalent to 60°) rotation about the *c*-axis in trigonal quartz (Frondel, 1945).

Dauphiné twins can form in response to deviatoric stresses (e.g. Lloyd, 2000; Pehl & Wenk, 2005; Thomas

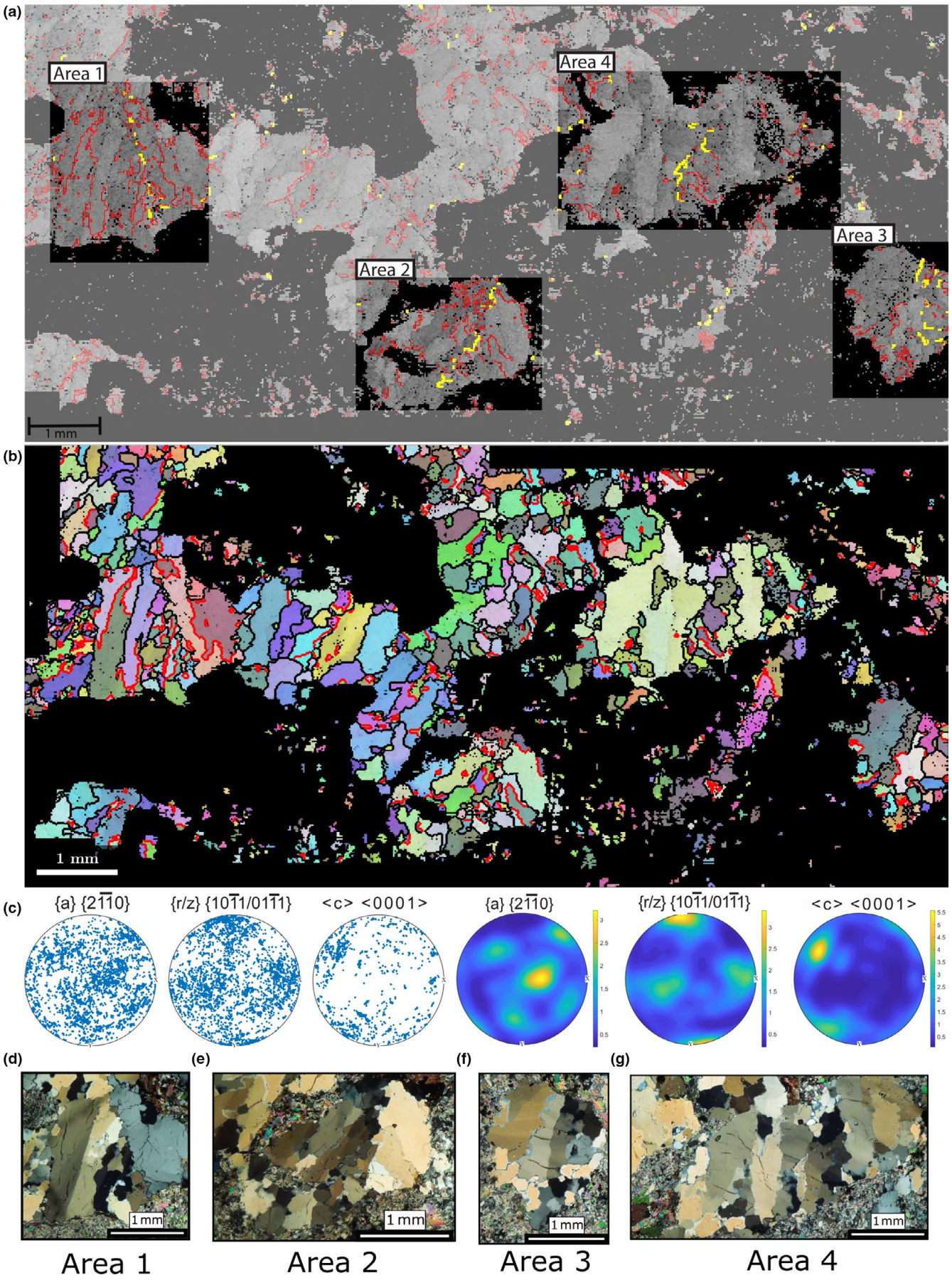

& Wooster, 1951; Tullis, 1970); however, the macroscopically undeformed nature of sample a05-10 and the different and unrelated crystallographic orientations between quartz domains makes this mechanism improbable. Instead, the presence of dauphiné twin-like relationships in sample a05-10 can be explained as a response to either: (1) beta- to alpha-quartz transition (Nord, 1994; Piazolo, Prior & Holness, 2005; Putnis, 1992); or (2) nucleation of quartz on to a coesite precursor. Given that pressure–temperature estimates from the Tso Morari dome record a retrograde path directly from the coesite stability field to that of alpha-quartz (Supporting Information 3), the beta–alpha-quartz transition can only explain the presence of dauphiné twin-like relationships if beta-quartz formed as a kinetically favoured metastable intermediate phase during nucleation and growth of alpha-quartz from coesite. There are currently no experimental observations which suggest whether or not the metastable nucleation of beta-quartz within the alpha-quartz stability field is possible and our study does not provide any observations that allow us to rule out this hypothesis, indicating that investigation is required. Alternatively, an alpha-quartz grain nucleating from coesite may adopt one of two orientations that are related to each other by the dauphiné twin law. This hypothesis also provides a viable explanation for the dauphiné twin-like misorientations along straight palisade grain boundaries in the Polokongka La sample, which is *atypical* for dauphiné twins that classically form irregular intragranular boundaries. Either hypothesis is consistent with our observations; further analyses would be required to identify which of those hypotheses is correct.

Our observations demonstrate a robust argument for a crystallographic control on the nucleation of palisade quartz from coesite. However, it is less clear whether this crystallographic control relates to either: (1) the orientation of the former coesite (i.e. an epitaxial nucleation), (2) the crystallographic or grain boundary orientations of the phase(s) surrounding the coesite or (3) is neither related to the former coesite nor the surrounding phase(s) (i.e. nucleation initiates in a random orientation but then proceeds in a crystallographically controlled orientation; e.g. Prior, David, Wheeler, Peruzzo, Spiess, & Storey, 2002).

In the case of the pyrope quartzite sample, quartz nucleation in the *c*-axis direction in subdomains 1 and 3 appears to have occurred perpendicular to adjacent inclusion boundary. Additionally, protrusions of palisade quartz into the coesite suggest quartz grains grew inwards from the inclusion walls into the coesite grain. These observations could indicate that a causative relationship exists between the inclusion boundary orientation and palisade quartz nucleation; however, such a hypothesis cannot explain the orientation of subdomain 2, in which the trace of the *c*-axis point maximum is aligned parallel to the inclusion boundary.

Hypotheses (2) and (3) for quartz nucleation also fail to explain the 90°/<*a*> misorientation between adjacent subdomains, observed in both samples. In the Polokongka La granite sample, large portions of the subdomain boundaries are coincident with a subdomain misorientation angle/axis pair of 90°/[02−21](yellow lines in Figure 7a), which approximates the (021) twin plane in coesite (Jacob, Cordier, Morniroli, & Schertl, 2009; Schertl et al., 1991). Additionally, coesite may also twin along the (100) and (−101) planes, which intersect (021) twins at 90° (e.g. Schertl, Medenbach, & Neuser, 2005). We therefore postulate that the formation of two quartz subdomains misoriented by 90°/<*a*> with respect to each other and bisected by a boundary with an orientation equivalent to twinning in coesite, as observed in the pyrope quartzite sample (Figure 3b), may have been controlled by the orientation of one or more twin planes in the former coesite. This would imply that the nucleation of palisade quartz was crystallographically controlled by the orientation of the former coesite grain.

An obvious test of this hypothesis is to consider the orientation of the coesite grain in the pyrope quartzite with respect to the surrounding palisade quartz. In this sample, coesite is untwinned in this section plane. However, quartz *c*-axis point maxima lie 90° apart on a plane that is parallel to the (101) plane (yellow great circle, Figure 3b) in the coesite inclusion, and bisected by the (−101) twin plane in the coesite inclusion (yellow dashed great circle, Figure 5b). We suggest that adjacent quartz subdomains epitaxially nucleated on adjacent sides of the (−101) coesite twin plane, implying that even in the absence of twinning, the coesite (−101) twin plane has a crystallographic control on the nucleation of quartz. As such, we suggest that the misorientations of adjacent palisade quartz subdomains may be explained by the crystallographic control of twin planes in former coesite on quartz nucleation and implies that the orientation of palisade quartz nucleation is epitaxially controlled by the orientation of the former coesite grain. Further investigation of palisade quartz surrounding twinned coesite grains would provide a valuable test of this hypothesis.

FIGURE 6 (a) Band contrast map showing targeted areas. Misorientations of 60°/[0001] are shown as red lines and misorientations of 90°/[02−21] are shown as yellow lines. The yellow lines are not continuous but define the boundary between texturally distinct subdomains of palisade quartz grains within each larger encompassing domain. (b) Euler map showing orientation of quartz grains. Red lines as in (a). (c) Uncontoured and contoured pole figure showing quartz orientations for the entire map area. (d–g) Photomicrographs of areas 1–4 [Colour figure can be viewed at wileyonlinelibrary.com]

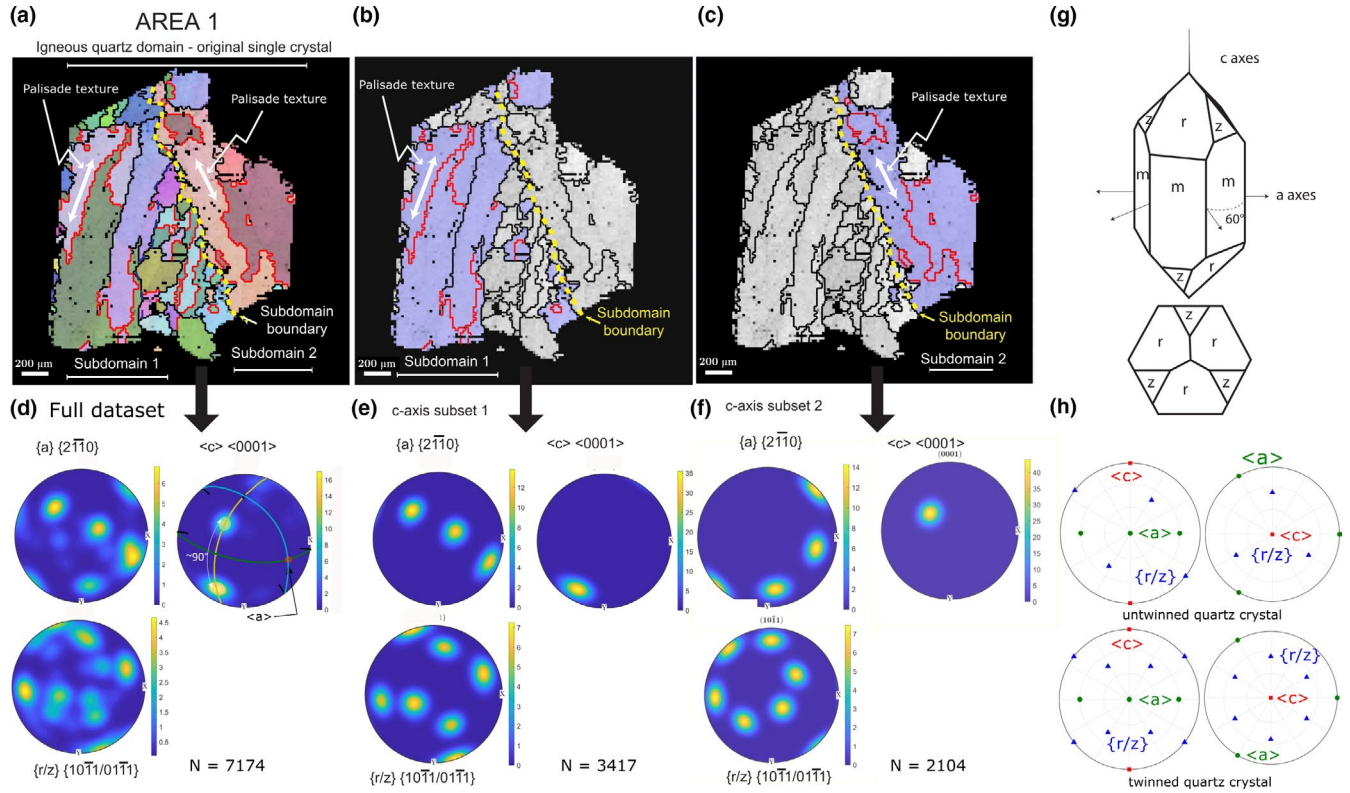

FIGURE 7 Results of EBSD and misorientation analysis of Area 1. Data for Areas 2, 3 and 4 in Supporting Information 2. All pole figures are lower hemisphere projections. Step size 20 µm. (a) Euler map showing orientation of individual grains. White arrows show the general orientation of quartz grains in each subdomain. Yellow line marks the boundary between subdomains with different *c*-axis orientations. Misorientations of 60° around [0001] are shown as red lines. (b) Subdomain 1 band contrast and grain boundary map showing the grains corresponding to the c-axis orientation in e (purple). (c) Subdomain 2 band contrast and grain boundary map showing the grains corresponding to the *c*-axis orientation in f (purple). (d) Pole figure of full domain showing [*c*] [0001] axis and <*a*><2−110> and {*r*/*z*} {10−11}/{01−11} planes. Distinct *c*-axis clusters plot along a single great circle with a relative orientation of 90°/<*a*>. (e) Pole figure of subdomain 1. Subsets defined by *c*-axis clusters shown in (d). (f) Pole figure of subdomain 2. Subsets defined by *c*-axis clusters shown in d. For further EBSD subsets of sample a05-10 see Supporting Information 2. (g) Schematic cartoon of an ideal untwinned quartz crystal. (h) Schematic pole figure for a single crystal of quartz with a vertical *c*-axis showing 6 *a*-axes around *c*-axis at 60° to each other and the poles to 3 *r*/*z* planes around the *c*-axis at 134° to each other [Colour figure can be viewed at wileyonlinelibrary.com]

5.2 | Further remarks on the preservation of palisade quartz textures in the Polokongka La granite

The preservation of microstructures after coesite confirms that sample a05-10 from the centre of the Tso Morari complex was subducted to UHP. However, microstructures after coesite are not a common feature in the granites of the Tso Morari dome and single igneous quartz crystals, which did not undergo transformation to coesite, are observed in other samples from within the Polokongka La region (Figure 3).

Transformation of quartz to coesite is a polymorphic reaction that not only has small uncertainties on the pressure at which it occurs but also is thought to take place relatively quickly in relation to geological timescales (Bohlen & Boettcher, 1982; Mosenfelder & Bohlen, 1997). Similarly, the reverse reaction is thought to take place relatively quickly such that coesite is rarely preserved in UHP rocks due to its low preservation potential (Mosenfelder & Bohlen, 1997). Based on the fast kinetics of the quartz–coesite and coesite–quartz reactions, it is puzzling as to why quartz palisade textures are not widely observed across the Polokongka La region given that the distribution of mafic eclogite pods imply that the whole of this region subducted to the coesite stability field. We suggest that the scarcity of quartz-after-coesite microstructures in the Polokongka La granite may be explained in a number of ways, of which we present three possibilities: (1) unidentified shear zones may subdivide the Tso Morari complex into regions with differing metamorphic histories, some of which may not have experienced UHP conditions; (2) the peak pressure experienced by the Tso Morari complex during subduction may have been equivalent to conditions at or just below the quartz–coesite transition, such that small variations in tectonic overpressure may have pushed some regions into the coesite stability field; and (3) factors such as deformation (i.e. differential stress) or fluid interaction may

be required to facilitate the quartz to coesite transition (e.g. Mosenfelder & Bohlen, 1997; Perrillat et al., 2003), such that the absence of deformation or fluid interaction (as indicated by petrographic observations of the Polokongka La granite) may permit the metastable persistence of quartz within the coesite stability field. Given the widespread evidence for UHP metamorphism recorded by the mafic eclogite pods from across the Tso Morari complex, we favour hypotheses (2) and (3).

5.3 | Implications for the investigation of continental subduction to UHP conditions

The formation and preservation of peak metamorphic textures in UHP terranes depends on: (1) stresses, temperature and availability of fluids needed to mediate prograde metamorphic reactions at UHP conditions (e.g. Austrheim, 1987; Terry & Heidelbach, 2006); and (2) a lack of exhumation-related deformation and metamorphism that would otherwise overprint and remove any record of peak conditions (e.g. Palin, St-Onge, Waters, Searle, & Dyck, 2014). UHP indicators may therefore be easier to find in the least deformed regions of a UHP terrane, such as low-strain granitic and mafic boudins and inclusions in rigid host minerals (e.g. Palin et al., 2014). Low-strain regions, such as the Polokongka La region of the Tso Morari complex, have not been comprehensively studied in any UHP terrane and may provide occurrences of matrix-scale palisade quartz textures in targeted sampling campaigns. Matrix palisade textures could also be readily mistaken for a deformation-related shape fabric, raising the possibility that some occurrences of UHP conditions have been overlooked, or misidentified.

In other UHP terranes, evidence of transformation of mineral assemblages at UHP conditions is typically widespread but not abundant (Cuthbert, Carswell, Krogh-Ravna, & Wain, 2000). Coesite inclusions are rare and difficult to find whereas polycrystalline quartz is a relatively common inclusion mineral (Cuthbert et al., 2000; Gilotti & Krogh Ravna, 2002; McClelland, Power, Gilotti, Mazdab, & Wopenka, 2006), suggesting a potentially more widespread occurrence of UHP conditions. For example, the Western Gneiss Region of Norway is a ~5,000 km^2 well-studied UHP terrane with only 15 confirmed occurrences of coesite and microdiamond that are considered indigenous to the crust and many reported occurrences of polycrystalline quartz inclusions (Butler, Jamieson, Steenkamp, & Robinson, 2013; Carswell et al., 2001; Carswell, Tucker, O'Brien, & Krogh, 2003; Cuthbert et al., 2000; Root et al., 2005; Smith, 1984; Smith & Lappin, 1989; Wain, 1997; Wain, Waters, Jephcoat, & Olijynk, 2000; Vrijmoed, Smith & Van Roermund, 2006; Schönig, Meinhold, von Eynatten, & Lünsdorf, 2018). In the Greenland Caledonides, coesite inclusions have only been found within zircon from a single outcrop, whereas polycrystalline quartz inclusions have been reported from multiple outcrops (McClelland et al., 2006).

The above-mentioned occurrences of quartz-after-coesite microstructures are based on *qualitative* assessments of optically visible microstructures. Our observations provide a *quantitative*, crystallographically defined set of criteria by which quartz-after-coesite microstructures may be identified and used as an indicator of UHP conditions. These repeatable observations can be summarized as follows: (1) quartz crystallographic orientations form multiple populations with 'single crystal' orientations defined by distinct *c*-axis point maxima; (2) Each 'single crystal' population of orientation measurements defines a spatially and texturally distinct subdomain of palisade quartz grains; (3) within each subdomain, apparent palisade quartz grain boundaries are subparallel to the trace of the *c*-axis orientation; (4) within each subdomain, misorientations of 60°/[0001] are recorded along anastomosing intragranular boundaries, whereas *r*- and *z*-poles to planes each form six point maxima around a single *c*-axis orientation; (5) adjacent subdomains are misoriented with respect to each other by a misorientation angle/axis pair of 90°/<*a*>; and (6) all *c*-axis point maxima from a single domain fall on a great circle that is approximately perpendicular to the <*a*> axis.

EBSD analyses of other occurrences of UHP rocks would help assess to ubiquity of our proposed UHP criteria. However, we stress the point that the repeatability of our observations from two isolated and unrelated UHP terranes strongly support the use of our observations as a robust and reliable indicator of quartz-after-coesite microstructures.

6 | CONCLUSIONS

The occurrence of UHP conditions in continental terranes continues to drive debate over the extent and mechanisms by which continental crust may be subducted and exhumed during continental collision (e.g. Hacker & Gerya, 2013; Parsons et al., 2020; Warren, 2013), and the importance of this process for orogenic cycles (e.g. Afonso & Zlotnik, 2011; Capitanio et al., 2010). In the absence of metamorphic reactions at high pressures, such as in felsic lithologies (e.g. O'Brien, 2018), evidence for subduction to UHPs is entirely dependent on the identification of poorly preserved coesite and the qualitative identification of quartz microstructures after coesite (Chopin, 1984; Smith, 1984). This study defines a set of crystallographic criteria in quartz after coesite, which can be used as a quantitative indicator of UHP conditions.

Our findings document several previously unreported textural observations by combining optical microscopy, EBSD and misorientation analysis. Our observations of

spatially and texturally distinct subdomains of palisade quartz textures with 'single crystal' orientations oriented at 90°/<*a*>, which formed during crystallographically controlled nucleation and growth of palisade quartz, may be a common and defining feature of quartz after coesite. In the absence of coesite, these features may represent the only quantitative indicator of UHP conditions in felsic lithologies.

The crystallographic patterns that we observe in the Dora Maira and Tso Morari samples provide the first quantitative approach of using CPO to identify and define palisade quartz textures. We believe that our observations are also the first reported evidence of crystallographic inheritance during the coesite to quartz reverse transformation and support the hypothesis by Langenhorst and Poirier (2002) for the exploitation of potential twin planes in former coesite during the nucleation of quartz. The repeatability of our observations in two unrelated occurrences of UHP rocks strongly supports our interpretation of a crystallographic control on the coesite to quartz transformation and the use of our reported observations as a quantitative indicator for UHP conditions. Such observations are an important addition to interpreting the numerous qualitative examples of palisade quartz inclusions, as well as the limited examples of palisade quartz textures in the matrix of natural samples. They also provide a useful indicator of burial to UHP conditions in terranes where coesite preservation is limited or absent. Further testing of our proposed UHP indicator should be recognized as an essential target for future studies of orogenesis and continental subduction, particularly in low-strain enclaves of felsic and siliceous rocks of continental terranes.

ACKNOWLEDGEMENTS

This work was funded by the Natural Environmental Research Council, grant number NE/L002612/1 awarded to AKB. Fieldwork to Ladakh was undertaken in 2016 and 2017 as part of the PhD of AKB and was partially funded by the Geological Society of London Mike Coward fund, the Mineralogical Society, Edinburgh Geological Society, University College Oxford and the Royal Geographical Society. RMG acknowledges funding from by the Natural Environmental Research Council, grant number NE/L002612/1. Sample DW09-53 was collected on the 2009 field excursion, led by Philippe Agard, funded through a joint France-UK academic exchange programme grant entitled 'The Hubert Curien Partnership (HCP) Alliance programme', awarded to P. Agard and C.-J. De Hoog. Thanks to Jon Wade and Phil Gopon from Oxford University for help and training on the SEM. Thanks to Katherine Kumamoto for writing the MTEX script for plotting EBSD data. Thanks also to Andrew Cross and anonymous reviewer number 2 for a constructive first review of the paper.

ORCID

Anna K. Bidgood https://orcid.org/0000-0001-7750-9524
Andrew J. Parsons https://orcid.org/0000-0001-7538-9418
Geoffrey E. Lloyd https://orcid.org/0000-0002-7859-2486
Dave J. Waters https://orcid.org/0000-0001-9105-9953
Rellie M. Goddard https://orcid.org/0000-0002-9805-1871

REFERENCES

Afonso, J. C., & Zlotnik, S. (2011). The subductability of continental lithosphere: The before and after story. In D. Brown & P. D. Ryan (Eds.), *Arc-continent collision*. Berlin, Heidelberg: Springer, Berlin Heidelberg.

Austrheim, H. (1987). Eclogitization of lower crustal granulites by fluid migration through shear zones. *Earth and Planetary Science Letters*, *81*(2–3), 221–232.

Avigad, D., Chopin, C., & Le Bayon, R. (2003). Thrusting and extension in the southern Dora-Maira ultra-high-pressure massif (Western Alps): View from below the coesite-bearing unit. *The Journal of Geology*, *111*, 57–70. https://doi.org/10.1086/344664

Bachmann, F., Hielscher, R., & Schaeben, H. (2010). Texture analysis with MTEX – free and open source software toolbox. *Solid state phenomena*, *160*, 63–68. https://doi.org/10.4028/www.scientific.net/SSP.160.63

Berthelsen, A. (1953). On the geology of the Rupshu District, NW Himalaya: A contribution to the problem of the Central Gneisses. *Meddelelser Fra Dansk Geologisk Forening (Kobenhavn)*, *12*, 351–414.

Bidgood, A. K., & Waters, D. J. (2019). The secret life of granite: A story of emplacement, alteration, subduction and metamorphism. *Applied Earth Science*, *128*(2), 38.

Bidgood, A., Waters, D., Searle, M., Roberts, N., & Ahmad, T. (2018). The Transformation History of the Tso Morari dome, Ladakh. *EGU General Assembly Conference Abstracts*, *20*, 137. https://meetingorganizer.copernicus.org/EGU2018/EGU2018-137-1.pdf.

Bohlen, S. R., & Boettcher, A. L. (1982). The quartz⇆ coesite transformation: A precise determination and the effects of other components. *Journal of Geophysical Research: Solid Earth*, *87*, 7073–7078.

Butler, J. P., Jamieson, R. A., Steenkamp, H. M., & Robinson, P. (2013). Discovery of coesite-eclogite from the Nordøyane UHP domain, Western Gneiss Region, Norway: Field relations, metamorphic history, and tectonic significance. *Journal of Metamorphic Geology*, *31*(2), 147–163. https://doi.org/10.1111/jmg.12004

Capitanio, F. A., Morra, G., Goes, S., Weinberg, R. F., & Moresi, L. (2010). India-Asia convergence driven by the subduction of the greater Indian continent. *Nature Geoscience*, *3*, 136. https://doi.org/10.1038/ngeo725

Carswell, D. A., Brueckner, H. K., Cuthbert, S. J., Krogh, T. E., Mehta, K., O'Brien, P. J., … Tucker, R. D. (2001). Coesite preservation within zircons in the Hareidland eclogite and the timing of ultra-high pressure metamorphism in the Western Gneiss Region of Norway. In *Fluid/slab/mantle interactions and ultrahigh-P minerals: UHPM workshop (extended abstracts)* (pp. 111–115).

Carswell, D. A., Tucker, R. D., O'Brien, P. J., & Krogh, T. E. (2003). Coesite micro-inclusions and the U/Pb age of zircons from the Hareidland Eclogite in the Western Gneiss Region of Norway. *Lithos*, *67*(3–4), 181–190. https://doi.org/10.1016/S0024-4937(03)00014-8

Chopin, C. (1984). Coesite and pure pyrope in high-grade blueschists of the Western Alps: A first record and some consequences. *Contributions to Mineralogy and Petrology*, *86*(2), 107–118. https://doi.org/10.1007/BF00381838

Chopin, C., & Schertl, H. P. (1999). The UHP unit in the Dora-Maira Massif, Western Alps. *International geology review*, *41*(9), 765–780.

Compagnoni, R., & Rolfo, F. (2003). UHPM units in the Western Alps. *Ultrahigh Pressure Metamorphism*, *5*, 13–49.

Compagnoni, R., Rolfo, F., Groppo, C., Hirajima, T., & Turello, R. (2012). Geological map of the ultra-high pressure Brossasco-Isasca unit (Western Alps, Italy). *Journal of Maps*, *8*(4), 465–472. https://doi.org/10.1080/17445647.2012.744367

Cuthbert, S. J., Carswell, D. A., Krogh-Ravna, E. J., & Wain, A. (2000). Eclogites and eclogites in the Western Gneiss region, Norwegian Caledonides. *Lithos*, *52*(1–4), 165–195. https://doi.org/10.1016/S0024-4937(99)00090-0

Epard, J., & Steck, A. (2008). Structural development of the Tso Morari ultra-high pressure nappe of the Ladakh Himalaya. *Tectonophysics*, *451*(1–4), 242–264. https://doi.org/10.1016/j.tecto.2007.11.050

Frondel, C. (1945). Secondary Dauphiné twinning in quartz. *American Mineralogist: Journal of Earth and Planetary Materials*, *30*(5–6), 447–460.

Gebauer, D. H. P. S., Schertl, H. P., Brix, M., & Schreyer, W. (1997). 35 Ma old ultrahigh-pressure metamorphism and evidence for very rapid exhumation in the Dora Maira Massif, Western Alps. *Lithos*, *41*(1–3), 5–24. https://doi.org/10.1016/S0024-4937(97)82002-6

Germain, L., Kratsch, D., Salib, M., & Gey, N. (2014). Identification of sub-grains and low angle boundaries beyond the angular resolution of EBSD maps. *Materials Characterization*, *98*, 66–72. https://doi.org/10.1016/j.matchar.2014.10.007

Gilotti, J. A., & Krogh Ravna, E. J. (2002). First evidence for ultrahigh-pressure metamorphism in the North-East Greenland Caledonides. *Geology*, *30*(6), 551. 10.1130/0091-7613(2002)030<0551:FEFUPM>2.0.CO;2

Girard, M., & Bussy, F. (1999). Late Pan-African magmatism in the Himalaya: New geochronological and geochemical data from the Ordovician Tso Morari metagranites (Ladakh, NW India). *Schweizerische Mineralogische Und Petrographische Mitteilungen*, *79*, 399–418.

Green, H. W., Griggs, D. T., & Christie, J. M. (1970). Syntectonic and annealing recrystallization of fine-grained quartz aggregates. *Experimental and Natural Rock Deformation [Experimentelle und Natürliche Gesteinsverformung]*, 272–335.

Guillot, S., Sigoyer, J. D., & Lardeaux, J. (1997). Eclogitic metasediments from the Tso Morari area (Ladakh, Himalaya): Evidence for continental subduction during India-Asia convergence. *Contributions to Mineralogy and Petrology*, *128*(2–3), 197–212.

Hacker, B. R., & Gerya, T. V. (2013). Paradigms, new and old, for ultrahigh-pressure tectonism. *Tectonophysics*, *603*, 79–88. https://doi.org/10.1016/j.tecto.2013.05.026

Hippert, J. F. (1994). Microstructures and c-axis fabrics indicative of quartz dissolution in sheared quartzites and phyllonites. *Tectonophysics*, *229*, 141–163. https://doi.org/10.1016/0040-1951(94)90026-4

Ihinger, P. D., & Zink, S. I. (2000). Determination of relative growth rates of natural quartz crystals. *Nature*, *404*, 865–869. https://doi.org/10.1038/35009091

Jacob, D., Cordier, P., Morniroli, J.-P., & Schertl, H.-P. (2009). Application of precession electron diffraction to the characterization of (021) twinning in pseudo-hexagonal coesite. *American Mineralogist*, *94*, 684–692. https://doi.org/10.2138/am.2009.3059

Langenhorst, F., & Poirier, J. P. (2002). Transmission electron microscopy of coesite inclusions in the Dora Maira high-pressure metamorphic pyrope-quartzite. *Earth and Planetary Science Letters*, *203*(3–4), 793–803. https://doi.org/10.1016/S0012-821X(02)00949-4

Lenze, A., & Stöckhert, B. (2007). Microfabrics of UHP metamorphic granites in the Dora Maira Massif, western Alps – No evidence of deformation at great depth. *Journal of Metamorphic Geology*, *25*(4), 461–475. https://doi.org/10.1111/j.1525-1314.2007.00707.x

Lenze, A., & Stöckhert, B. (2008). Microfabrics of quartz formed from coesite (Dora-Maira Massif, Western Alps). *European Journal of Mineralogy*, *20*(5), 811–826. https://doi.org/10.1127/0935-1221/2008/0020-1848

Lloyd, G. E. (2000). Grain boundary contact effects during faulting of quartzite: An SEM/EBSD analysis. *Journal of Structural Geology*, *22*(11–12), 1675–1693. https://doi.org/10.1016/S0191-8141(00)00069-9

Mainprice, D., Bachmann, F., Hielscher, R., & Schaeben, H. (2014). Descriptive tools for the analysis of texture projects with large datasets using MTEX: Strength, symmetry and components Rock Deformation from Field. In *Experiments and Theory: A Volume in Honour of Ernie Rutter*.

McClelland, W., Power, S., Gilotti, J., Mazdab, F., & Wopenka, B. (2006). U-Pb SHRIMP geochronology and trace-element geochemistry of coesite-bearing zircons, North-East Greenland Caledonides. *Special Papers – Geological Society of America*, *403*, 23.

Nord, G. L. (1994). Transformation-induced twin boundaries in minerals. *Phase Transitions*, *48*(1–3), 107–134. https://doi.org/10.1080/01411599408200356

O'Brien, P. J. (2018). Tso Morari coesite eclogite: Pseudosection predictions v. the preserved record and implications for tectonometamorphic models. *Geological Society, London, Special Publications*, *474*(1), 5–24. https://doi.org/10.1144/SP474.16

O'Brien, P. J. (2006). The age of deep, steep continental subduction in the NW Himalaya: Relating zircon growth to metamorphic history. Comment on:"The onset of India-Asia continental collision: Early, steep subduction required by the timing of UHP metamorphism in the western Himalaya" by Mary L. Leech, S. Singh, AK Jain, Simon L. Klemperer and RM Manickavasagam, Earth and Planetary Science Letters 234 (2005) 83–97. *Earth and Planetary Science Letters*, *245*(3–4), 814–816.

O'Brien, P. J., Zotov, N., & Law, R. (1999). First discovery of coesite in the Kaghan eclogites (Pakistan): Implications for Himalayan evolution. *Terra Nova*, *2*, 109–111.

Okay, A., Xu, S., & Sengor, A. (1989). Coesite from the Dabie Shan eclogites, central China. *European Journal of Mineralogy*, *1*(4), 595–598.

Palin, R. M., Reuber, G. S., White, R. W., Kaus, B. J., & Weller, O. M. (2017). Subduction metamorphism in the Himalayan ultrahigh-pressure Tso Morari massif: An integrated geodynamic and petrological modelling approach. *Earth and Planetary Science Letters*, *467*, 108–119. https://doi.org/10.1016/j.epsl.2017.03.029

Palin, R. M., St-Onge, M. R., Waters, D. J., Searle, M. P., & Dyck, B. (2014). Phase equilibria modelling of retrograde amphibole and clinozoisite in mafic eclogite from the Tso Morari massif, northwest India: Constraining the P-T-M (H_2O) conditions of exhumation. *Journal of Metamorphic Geology*, *32*(7), 675–693. https://doi.org/10.1111/jmg.12085

Parsons, A. J., Hosseini, K., Palin, R., & Sigloch, K. (2020). Geological, geophysical and plate kinematic constraints for models of the India-Asia collision and the post-Triassic central Tethys oceans. *Earth-Science Reviews*, 103084. https://doi.org/10.1016/j.earscirev.2020.103084

Passchier, C. W., & Trouw, R. A. (2005). *Microtectonics*. Berlin Heidelberg: Spinger.

Pehl, J., & Wenk, H. R. (2005). Evidence for regional Dauphiné twinning in quartz from the Santa Rosa mylonite zone in Southern California. A neutron diffraction study. *Journal of Structural Geology*, *27*(10), 1741–1749. https://doi.org/10.1016/j.jsg.2005.06.008

Perrillat, J. P., Daniel, I., Lardeaux, J. M., & Cardon, H. (2003). Kinetics of the coesite–quartz transition: Application to the exhumation of ultrahigh-pressure rocks. *Journal of Petrology*, *44*(4), 773–788. https://doi.org/10.1093/petrology/44.4.773

Philippot, P., Chevallier, P., Chopin, C., & Dubessy, J. (1995). Fluid composition and evolution in coesite-bearing rocks (Dora-Maira massif, Western Alps): Implications for element recycling during subduction. *Contributions to Mineralogy and Petrology*, *121*(1), 29. https://doi.org/10.1007/s004100050088

Piazolo, S., Prior, D. J., & Holness, M. D. (2005). The use of combined cathodoluminescence and EBSD analysis: A case study investigating grain boundary migration mechanisms in quartz. *Journal of Microscopy*, *217*(2), 152–161. doi: 10.1111/j.1365-2818.2005.01423.x.

Prior, D. J., Wheeler, J., Peruzzo, L., Spiess, R., & Storey, C. (2002). Some garnet microstructures: An illustration of the potential of orientation maps and misorientation analysis in microstructural studies. *Journal of Structural Geology*, *24*(6–7), 999–1011. https://doi.org/10.1016/S0191-8141(01)00087-6

Putnis, A. (1992). *An introduction to mineral sciences*. Cambridge, UK: Cambridge University Press.

Root, D. B., Hacker, B. R., Gans, P. B., Ducea, M. N., Eide, E. A., & Mosenfelder, J. L. (2005). Discrete ultrahigh-pressure domains in the Western Gneiss Region, Norway: Implications for formation and exhumation. *Journal of Metamorphic Geology*, *23*(1), 45–61. https://doi.org/10.1111/j.1525-1314.2005.00561.x

Sachan, H. K., Mukherjee, B. K., Ogasawara, Y., Maruyama, S., Ishida, H., Muko, A., & Yoshioka, N. (2004). Discovery of coesite from Indus Suture Zone (ISZ), Ladakh, India: Evidence for deep subduction. *European Journal of Mineralogy*, *16*(2), 235–240. https://doi.org/10.1127/0935-1221/2004/0016-0235

Schertl, H. P., Medenbach, O., & Neuser, R. D. (2005). UHP-metamorphic rocks from Dora Maira, Western Alps: Cathodoluminescence of silica and twinning of coesite. *Russian Geology and Geophysics*, *46*(12), 1345–1351.

Schertl, H.-P., Schreyer, W., & Chopin, C. (1991). The pyrope-coesite rocks and their country rocks at Parigi, Dora Maira Massif, Western Alps: Detailed petrography, mineral chemistry and PT-path. *Contributions to Mineralogy and Petrology*, *108*(1–2), 1–21. https://doi.org/10.1007/BF00307322

Schönig, J., Meinhold, G., von Eynatten, H., & Lünsdorf, N. (2018). Tracing ultrahigh-pressure metamorphism at the catchment scale. *Scientific Reports*, *8*(1), 2931. https://doi.org/10.1038/s41598-018-21262-8

Sigoyer, J. D., Guillot, S., Lardeaux, J. M., & Mascle, G. (1997). Glaucophane-bearing eclogites in the Tso Morari dome (eastern Ladakh, NW Himalaya). *European Journal of Mineralogy*, 1073–1084.

Smith, D. C. (1984). Coesite in clinopyroxene in the Caledonides and its implications for geodynamics. *Nature*, *310*(5979), 641–644. https://doi.org/10.1038/310641a0

Smith, D. C., & Lappin, M. A. (1989). Coesite in the Straumen kyanite-eclogite pod, Norway. *Terra Nova*, *1*(1), 47–56. https://doi.org/10.1111/j.1365-3121.1989.tb00325.x

Steck, A., Epard, J. L., Vannay, J. C., Hunziker, J., Girard, M., Morard, A., & Robyr, M. (1998). Geological transect across the Tso Morari and Spiti areas: The nappe structures of the Tethys Himalaya. *Eclogae Geologicae Helvetiae*, *91*, 103–121.

St-Onge, M. R., Rayner, N., Palin, R. M., Searle, M. P., & Waters, D. J. (2013). Integrated pressure – temperature – time constraints for the Tso Morari dome (Northwest India): Implications for the burial and exhumation path of UHP units in the western Himalaya. *Journal of Metamorphic Geology*, *31*(5), 469–504. https://doi.org/10.1111/jmg.12030

Terry, M. P., & Heidelbach, F. (2006). Deformation-enhanced metamorphic reactions and the rheology of high-pressure shear zones, Western Gneiss Region, Norway. *Journal of Metamorphic Geology*, *24*(1), 3–18. https://doi.org/10.1111/j.1525-1314.2005.00618.x

Thakur, V. C. (1983). Deformation and metamorphism in the Tso Morari Crystalline Complex. In V. C. Thakur & K. K. Sharma (Eds.), *Geology of the Indus Suture Zone of Ladakh* (pp. 1–8). Dehra Dun, India: Wadia Institute of Himalayan Geology.

Thomas, L. A., & Wooster, W. A. (1951). Piezoerescence – The growth of Dauphiné twinning in quartz under stress. *Proceedings of the Royal Society of London. Series A. Mathematical and Physical Sciences*, *208*(1092), 43–62.

Tullis, J. (1970). Quartz: Preferred orientation in rocks produced by Dauphiné twinning. *Science*, *168*(3937), 1342–1344.

Vrijmoed, J., Smith, D., & Van Roermund, H. (2006). Microdiamond (in situ) in the Svartberget peridotite, Vestlandet, Norway, confirmed by Raman Microscopy. In *Geo-Raman '06, 7th International Conference on Raman Spectroscopy, Applied to Earth and Planetary Sciences* (pp. 85–86).

Wain, A. (1997). New evidence for coesite in eclogite and gneisses: Defining an ultrahigh-pressure province in the Western Gneiss region of Norway. *Geology*, *25*(10), 927–930. https://doi.org/10.1130/0091-7613(1997)025

Wain, A., Waters, D., Jephcoat, A., & Olijynk, H. (2000). The high-pressure to ultrahigh-pressure eclogite transition in the Western Gneiss Region, Norway. *European Journal of Mineralogy*, *12*(3), 667–687. https://doi.org/10.1127/0935-1221/2000/0012-0667

Warren, C. J. (2013). Exhumation of (ultra-)high-pressure terranes: Concepts and mechanisms. *Solid Earth*, *4*, 75–92. https://doi.org/10.5194/se-4-75-2013

SUPPORTING INFORMATION

Additional supporting information may be found online in the Supporting Information section.

Supporting Information 1. Geological map taken from St-Onge et al. (2013) after Epard and Steck (2008) and references therein

Supporting Information 2. Further EBSD subsets of sample a05-10. All pole figures are lower hemisphere projections. Areas 2, 3 and 4

Supporting Information 3. Summary of *P–T* results and proposed *P–T* paths for the Tso Morari eclogites after O'Brien (2018)

How to cite this article: Bidgood AK, Parsons AJ, Lloyd GE, Waters DJ, Goddard RM. EBSD-based criteria for coesite-quartz transformation. *J Metamorph Geol*. 2021;39:165–180. https://doi.org/10.1111/jmg.12566